

# Effect of depletion interactions on transport of colloidal particles in porous media

Paweł Weroński,<sup>1</sup> John Y. Walz,\* and Menachem Elimelech

*Department of Chemical Engineering, Yale University, P.O. Box 208286, New Haven, CT 06520-8286, USA*

Received 26 July 2002; accepted 5 February 2003

## Abstract

The influence of depletion interactions on the transport of micrometer-sized, negatively charged polystyrene latex particles through porous media was studied by analysis of particle breakthrough curves as a response to short-pulse particle injections to the inlet of a packed column of glass beads. The column outlet latex particle concentration profiles and the total amount of particles exiting the column were determined as a function of the concentration of small, silica nanoparticles in the solution and the bulk flow rate. Because of similar charges, the silica particles do not adsorb to either the latex particles or glass beads and thus induce an attractive depletion force between the latex particles and glass bead collectors. The total column outlet latex particle amount was calculated by integrating the measured breakthrough concentration curve and compared to the known amount of injected particles at the column inlet. It was found that the particle recovery was a decreasing function of the silica nanoparticle concentration and the carrier fluid residence time, and an increasing function of the velocity in the bed. In addition, removing the silica nanoparticles from the flowing solution caused a second outlet peak to appear, suggesting that some of the polystyrene particles were captured in secondary energy wells. The experimental data were interpreted using the predicted potential energy profile between a single particle and a glass bead, which was assumed to consist of electrostatic, van der Waals, and depletion components. The results indicate that secondary energy wells significantly affect particle transport behavior through porous media.

© 2003 Elsevier Science (USA). All rights reserved.

*Keywords:* Colloid transport; Particle adsorption; Reversible adsorption; Particle deposition; Colloidal forces; Depletion forces; Depletion interaction; Phase separation; Secondary minimum effect

## 1. Introduction

Depletion interaction arises from the presence of a smaller, nonadsorbing species in a particle suspension, such as polymer molecules, micelles, or other small nanoparticles. The origin of the interaction was first explained successfully by Asakura and Oosawa using the concept that the free volume available to nonadsorbing polymer molecules increases whenever two hard particles approach sufficiently close, which is energetically favorable [1]. Since this classic study, a substantial amount of theoretical and modeling work has been focused on the problem (reviews are given by Seebergh and Berg [2] and Jenkins and Snowden [3]). In addition, direct experimental measurement of the interaction has been obtained with a variety of techniques, including

the surface force apparatus [4], atomic force microscopy [5–8], total internal reflection microscopy [9–14], differential electrophoresis [15], optical tweezer methods [16], and the hydrodynamic force balance method [17].

The present paper focuses on the still unexplored effect of depletion interactions on the transport behavior of colloidal particles in porous media. The work is unique in that previous experimental studies have focused primarily on static systems (i.e., no bulk transport). The experiments also probe whether shallow, reversible, secondary energy wells can significantly alter the particle transport and retention behavior. One advantage of using depletion interactions to study this question is that the location and depth of the secondary energy well can be controlled via the size and concentration of the nonadsorbing species. In addition, because the depth of the secondary depletion well will depend on the physical properties of the particles (i.e., the size and charge density), depletion interactions could potentially be used to enhance the separation of particles in a packed bed. Specifically, particles that experience a larger attraction (and hence deeper

\* Corresponding author.

*E-mail address:* [john.walz@yale.edu](mailto:john.walz@yale.edu) (J.Y. Walz).

<sup>1</sup> On leave from the Institute of Catalysis and Surface Chemistry, Polish Academy of Sciences, ul. Niezapominajek 8, 30-239 Kraków, Poland.

secondary energy well) would travel through the bed more slowly than particles experiencing a weaker attraction.

The paper is organized as follows. An overview of the primary particle-collector interaction forces acting in our experimental system is first presented. The depletion interaction is modeled using the force-balance approach originally developed by Walz and Sharma [18] and later modified by Piech and Walz to include the effects of polydispersity [19] and shape [20] of the nonadsorbing material on the depletion interaction between two surfaces. This model assumes that all species interact through screened electrostatic forces and uses a second-order virial expansion to calculate the radial distribution of the nonadsorbing material around the particles and surfaces. We then present a series of experiments in which pulses of micrometer-sized polystyrene spheres are transported through a packed bed of spherical glass beads (collectors) in the presence of various concentrations of nanometer-sized silica colloids. Because of the negative charge present on all surfaces, minimal adsorption of the silica occurs to either the polystyrene or glass, producing a depletion interaction between the particles and collectors. Latex particle breakthrough concentrations were measured using a UV/Vis spectrophotometer in a flowthrough cell specially designed for colloidal applications. Experiments were also conducted at varying bulk flow rates to explore the effect of hydrodynamics and residence time on the fraction of particles captured. The breakthrough curves were analyzed qualitatively using the predicted particle-collector energy profiles.

## 2. Theory

The total interaction energy between a single particle and a spherical collector in the experiments described below consists of three primary components: a screened electrostatic repulsion arising from the charged surfaces, an attractive van der Waals (London dispersion) interaction, and a depletion/structural interaction produced by the presence of the nonadsorbing nanoparticles. Thus

$$E(h) = E_{\text{elect}}(h) + E_{\text{vdw}}(h) + E_{\text{dep}}(h), \quad (1)$$

where  $h$  represents the gap width between a single particle and a collector. We assume here that the interaction between a particle and a collector is unaffected by the presence of other particles (i.e., the energies are a function only of the particle-collector gap width), which is valid for relatively low particle concentrations.

We will model all electrostatic interactions in the system using the linear superposition approximation (LSA) of Bell et al. [21]. For two spherical particles of radii  $a_i$  and  $a_j$ , separated by gap width  $h$ , the repulsive energy is

$$E_{\text{elec}}(h) = 4\pi\epsilon_r\epsilon_0\left(\frac{kT}{e}\right)^2 Y_i Y_j \frac{a_i a_j}{r} \exp(-\kappa h), \quad (2)$$

where  $r$  is the center-to-center distance between the spheres ( $r = h + a_i + a_j$ ),  $\epsilon_r$  is the relative dielectric constant of the medium,  $\epsilon_0$  is the permittivity of free space,  $e$  is the electron charge,  $\kappa^{-1}$  is the Debye length, and  $Y_i$  and  $Y_j$  are the effective surface potentials of particles  $i$  and  $j$ , respectively (the definition of the effective surface potential is given in Bell et al.). As stated by the authors, this equation is believed to be the correct limiting form of the potential at large values of  $\kappa h$  for all surface potentials, particle radii, and electrolyte types, provided that the correct values of  $Y_i$  and  $Y_j$  are used. Even though the LSA method tends to slightly overestimate the interaction energy at smaller separations, Bell et al. state that at separations of one Debye length and absolute surface potentials below 100 mV, the interaction energy predicted by Eq. (2) is within 10% of the true value. For our particular experiments, the electrostatic repulsive forces were sufficiently strong that the repulsive energies between all components exceeded the characteristic Brownian energy,  $kT$ , at separations larger than the bulk Debye length. Because of the dominance of Brownian relative to convective motion in the experiments, Eq. (2) is applicable here (i.e., all equilibrium separation distances are larger than the bulk Debye length).

The van der Waals attraction between the particle and the collector was calculated as

$$E_{\text{vdw}}(h) = -\frac{1}{6}\left(\frac{a_p a_c}{a_p + a_c}\right) \int_h^\infty \frac{A(h')}{h'^2} dh', \quad (3)$$

where  $A$  is the Hamaker constant for the interaction between two planar half-spaces separated by gap width  $h'$ . This parameter was calculated here using the Lifshitz continuum theory with the appropriate dielectric spectra data taken from Parsegian and Weiss [22]. Equation (3) uses the Derjaguin approximation to account for the effect of the curvature of the particle and collector surfaces, which is valid in these experiments because of the relatively large size of the particles (0.96  $\mu\text{m}$  diameter) and collectors (300  $\mu\text{m}$  diameter).

The depletion interaction between a particle and collector was calculated using the force-balance model originally developed by Walz and Sharma [18] and later modified by Piech and Walz [19,20]. We provide here a basic overview of the model. A spherical particle of radius  $a_p$  interacts with a much larger spherical collector of radius  $a_c$  across a gap width  $h$  (see Fig. 1). The equilibrium system also contains spherical, nonadsorbing depletant particles of radius  $a_d$  at a bulk number concentration,  $\rho_\infty$ . The total force exerted on the particle by the surrounding nanoparticles can be written as

$$\mathbf{F}_{\text{dep}}(\mathbf{r}_{\text{cp}}) = - \int_{r_{\text{pd}}} \rho(\mathbf{r}_{\text{pd}}, \mathbf{r}_{\text{cd}}) \nabla E_{\text{pd}}(\mathbf{r}_{\text{pd}}) d\mathbf{r}_{\text{pd}}, \quad (4)$$

where  $\rho(\mathbf{r}_{\text{pd}}, \mathbf{r}_{\text{cd}})$  is the number density of the depletant particles at some point in the fluid and  $\nabla E_{\text{pd}}(\mathbf{r}_{\text{pd}})$  is the gradient of the interaction energy between a single particle and a depletant. The integration in this equation is performed

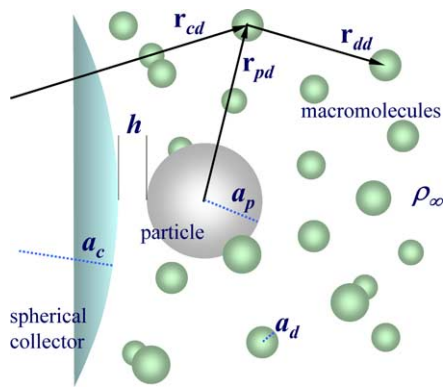


Fig. 1. Schematic representation of a spherical particle of radius  $a_p$  and a spherical collector of radius  $a_c$  interacting across gap width  $h$  in a solution containing spherical nonadsorbing particles of radius  $a_d$  and bulk concentration  $\rho_\infty$ .

over the entire system volume. Note that the subscripts c, d, and p refer to the collector, depletant, and particle, respectively.

The interaction energy,  $E_{pd}(\mathbf{r}_{pd})$ , consists of a hard wall repulsion plus a screened electrostatic interaction given by Eq. (2). The density distribution,  $\rho(\mathbf{r}_{pd}, \mathbf{r}_{cd})$  was calculated using a second-order virial expansion of the form

$$\rho(\mathbf{r}_{pd}, \mathbf{r}_{cd}) = \rho_\infty \exp\{-[E_{pd}(\mathbf{r}_{pd}) + E_{cd}(\mathbf{r}_{cd})]\} \times [1 + b_2(\mathbf{r}_{pd}, \mathbf{r}_{cd}) + O(\rho_\infty^2)], \quad (5)$$

where  $E_{cd}$  is the interaction energy between a single depletant and a collector and  $b_2(\mathbf{r}_{pd}, \mathbf{r}_{cd})$  is the second virial coefficient for a depletant interacting simultaneously with a particle and a collector. This coefficient is the first correction in the virial expansion for interactions between the depletant particles themselves, which, again, are assumed to consist of screened electrostatic repulsions. Expression for  $b_2(\mathbf{r}_{pd}, \mathbf{r}_{cd})$  are given by Walz and Sharma [18].

Note that Weroński and Walz [23] showed that for systems where  $\kappa a_p \gg 1$  and  $\kappa a_c \gg 1$ , the virial coefficient for a depletant interacting with both a particle and a collector can be accurately approximated as the sum of the two coefficients calculated independently for the particle and collector (i.e., superposition of the virial coefficients), which is the approach used in the Walz and Sharma model. In addition, for sufficiently low depletant concentrations, we can assume that the interaction energies between a particle and a depletant,  $E_{pd}$ , and a collector and a nanoparticle,  $E_{cd}$ , are only function of the distance of separation. Thus  $E_{pd}(\mathbf{r}_{pd}) = E_{pd}(r_{pd})$  and  $E_{cd}(\mathbf{r}_{cd}) = E_{cd}(r_{cd})$ . Hence, the final expression for the depletion interaction is

$$\mathbf{F}_{\text{dep}}(\mathbf{r}_{cp}) = - \int_{\mathbf{r}_{pd}} \rho_\infty \exp\{-[E_{pd}(r_{pd}) + E_{cd}(r_{cd})]\} \times [1 + b_2(\mathbf{r}_{pd}, \mathbf{r}_{cd})] \nabla E_{pd}(r_{pd}) d\mathbf{r}_{pd}. \quad (6)$$

The corresponding depletion energy,  $E_{\text{dep}}(h)$ , can be calculated as

$$E_{\text{dep}}(h) = - \int_{\infty}^{r_{cp}} \mathbf{F}_{\text{dep}}(\mathbf{r}_{cp}) \cdot d\mathbf{r}_{cp}, \quad (7)$$

where  $h = r_{cp} - a_p - a_c$ .

There are a number of implicit assumptions in this approach that should be noted here. First, by modeling the electrostatic interactions using Eq. (2) and the bulk solution properties (i.e., bulk Debye screening length), we are assuming that the ionic atmosphere around the depletant particles is not disturbed by the presence of the other charged depletant particles and particles. This assumption should be valid provided  $\kappa a_d > 1$  ( $\kappa a_d$  is 1.8 in our experiments) and the effective depletant particle concentration (i.e., the volume occupied by the depletant particles plus the surrounding counterion cloud) is much less than 1. If we assume that the effective depletant particle radius is equal to  $a_d + \kappa^{-1}$ , then the highest effective volume fraction in our experiments was 0.15. The second assumption is related to our use of the superposition approximation, Eq. (5), which is valid for weakly overlapping double layers. Because of the relatively strong repulsive electrostatic energies in our system, the low effective volume fraction of depletant particles, and the fact that convection effects were negligible at the depletion interaction range (the thickness of the diffusion boundary layer was orders of magnitude greater than the range of surface forces), this assumption is valid.

### 3. Experimental

#### 3.1. Colloidal particles and granular porous media

Surfactant-free polystyrene latex particles containing sulfate surface functional groups (batch 1-1000, Interfacial Dynamics Corp., Portland, OR) and colloidal silica (Snowtex-O, Nissan Chemical Industries, LTD) were used as model colloids and depletant nanoparticles, respectively. The manufacturer-reported mean latex particle diameter was  $0.96 \pm 0.09 \mu\text{m}$  and the suspension concentration was 84 g/l. The silica nanoparticle size reported by the manufacturer was 11–14 nm. The silica suspension concentration was determined gravimetrically, yielding a volume fraction of  $9.0 \pm 0.9\%$ . A packed bed of soda lime glass beads (Class V, Ferro Corp., Jackson, MS), with an average diameter of 0.27 mm, was used as a granular porous medium.

#### 3.2. Characterization of particles and glass beads

The size and electrophoretic mobility of the latex particles were measured using a Brookhaven Instruments ZetaPALS (Brookhaven Instruments Corp., Holtsville, NY). A log-normal particle size distribution was assumed. The silica nanoparticle size and electrophoretic mobility were mea-

Table 1  
Size and zeta potential of the colloids and glass beads

Material	Concentration used in the size and zeta potential measurements, % vol	Measured diameter, $\mu\text{m}$	Measured zeta potential, mV
Polystyrene	$(4.0 \pm 0.05) \times 10^{-3}$	$0.96 \pm 0.03$	$-110 \pm 15$
Silica	$3.0 \pm 0.3$	$0.011 \pm 0.002$	$-57 \pm 2$
Glass beads	–	$300 \pm 30$	$-65 \pm 3$

sured using acoustic and electroacoustic spectroscopy (DT-1200, Dispersion Technology Inc., Mt Kisco, NY) which is more precise compared to the traditional light-based techniques for particles smaller than 100 nm [24]. A log-normal distribution for the nanoparticle sizes was also assumed. The zeta potentials of the latex particles and silica nanoparticles were calculated from the measured electrophoretic mobility values using the program of O'Brien and White [25].

The streaming potential of the granular porous medium was determined with a streaming potential analyzer (BI-EKA, Brookhaven Instruments Corp.). The analyzer was equipped with Ag–AgCl electrodes and a cylindrical cell with an inner diameter of 2.0 cm to house the granular porous medium. The bed length was 4 cm and the porosity was 0.37. The streaming potential was converted to zeta potential using the Helmholtz–Smoluchowski equation and the Fairbrother and Mastin approach [26].

The measured properties of the latex particles, silica nanoparticles, and glass bead collectors are summarized in Table 1. Note that all measurements were conducted in a solution having the same chemical composition as the solution used during the corresponding column experiments. The confidence intervals given here are the standard deviation in the measured values (note that the diameters of the polystyrene and silica spheres were assumed to be distributed log normally).

### 3.3. Column setup

In our experiments we adopted a chromatographic short-pulse technique first used for measuring colloid deposition by Kretzschmar et al. [27]. Colloid transport experiments were conducted by injecting a  $177.5 \pm 1.6 \mu\text{l}$  pulse of colloidal particle suspension (1 g/l) to the inlet of an adjustable-height glass chromatography column (Omnifit USA, Toms River, NJ) packed with clean glass beads (Fig. 2). The connection between the loop and the porous bed consisted of Teflon tubing (79 mm long, 0.8 mm i.d.) and a Teflon column endpiece (115 mm long, 1.5 mm i.d.). The column had an inner diameter of 1 cm. Polyethylene meshes (149  $\mu\text{m}$ ) were placed at both ends of the column. The porous medium was “wet-packed” in deionized water and then washed with a solution used during the subsequent transport experiment. The packing porosity for each experiment was determined to be  $0.37 \pm 0.01$  based on a glass bead

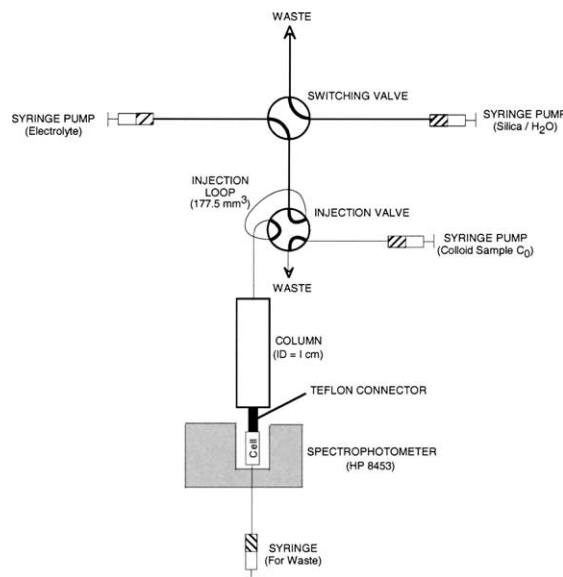


Fig. 2. Schematic of the column setup for particle transport experiments.

density of  $2.5 \text{ g/cm}^3$ . The bed length was  $14.8 \pm 0.2 \text{ cm}$ . A constant flow of either a background electrolyte solution or a solution of silica nanoparticles was delivered to the column by syringe pumps (Model 22, Harvard Apparatus, Inc., Hilliston, MA) at the specified flow velocity. A chemically inert 4-port switching valve (Model V-100D, Upchurch Scientific, Oak Harbor, WA) was used to switch between solutions smoothly. A Teflon low-pressure injection valve with continuous flow design (Model 5020, Supelco, Bellefonte, PA) was adopted to ensure accurate and smooth pulse injection of the particle suspension. The Teflon injection loop volume (i.d. 0.8 mm) was determined by measuring the mass of water injected to the loop, based on a known water temperature and density. The colloid concentration at the column outlet was monitored on-line with a UV/Vis spectrophotometer (Hewlett-Packard Model 8453) equipped with a flowthrough cell. The column apparatus and all accessories were carefully cleaned between experimental runs with a strong acid (HCl) followed by a final rinse with deionized water. Care was taken to prevent or remove air bubbles from the system, and the system was kept closed to prevent absorption of  $\text{CO}_2$ .

Three important modifications were introduced to the standard column setup to achieve improved reproducibility of the experimental results. First, the output of the system was closed with a syringe collecting the waste electrolyte. Thus the system had no open ends, which provided better pressure and flow stabilization. Second, the tubing between the column and the flowthrough cell was replaced with a short, stiff Teflon connector (Model P-645, Upchurch Scientific) to minimize hydrodynamic dispersion effects. Last, a new custom-made flowthrough cell was employed in the spectrophotometer.

Because standard flowthrough cells are designed primarily for measurement of molecular species, where the typical

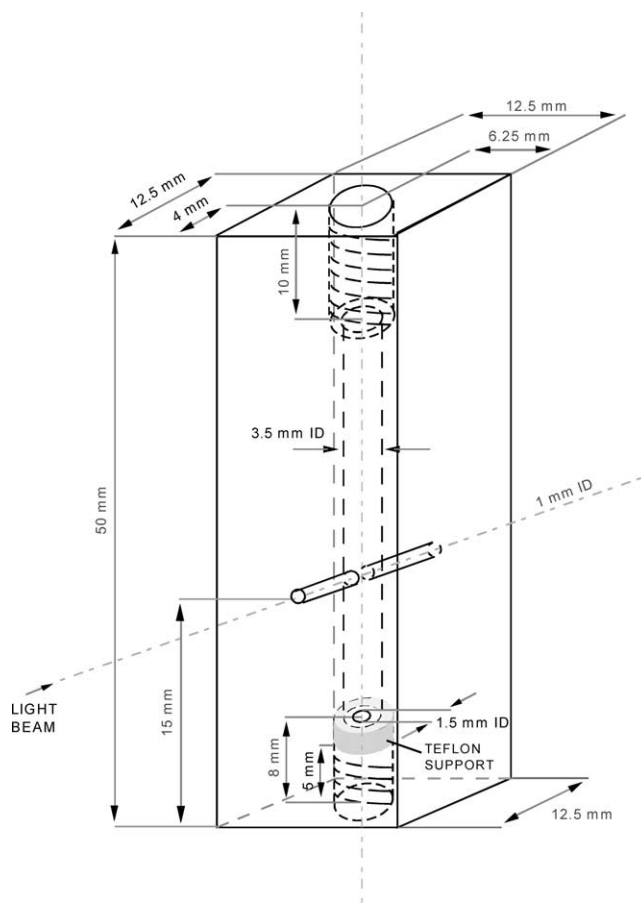


Fig. 3. Schematic of the custom-made flowthrough cell used in conjunction with a UV–Vis spectrophotometer to monitor the column outlet latex particle concentration.

diffusion time scale is orders of magnitude lower than that of colloidal particles, the geometry of a standard flowthrough cell, which has a sudden change in diameter at the inlet, leads to mixing problems in the cell. To overcome this problem, we designed a cell with cylindrical geometry and an inner diameter equal to the inner diameter of the column-cell Teflon connector (1.5 mm). The main part of this cell (Fig. 3) was a piece of quartz tubing (inner and outer diameters of 1.5 and 3.5 mm, respectively, and length 34 mm) installed inside of a piece of plastic (Black Darlin, 12.5 × 12.5 × 50.0 mm). A cylindrical cross-through hole (1 mm in diameter) at the center of the plastic block, 15 mm from the bottom, ensured correct illumination of the flowing suspension and served as the cell window. The total suspension path length between the column outlet and the cell window (column end-piece, column-cell connector, and quartz tubing) was 90 mm with a fixed inner diameter of 1.5 mm. The diameter of the window was somewhat smaller (67%) than the inner diameter of the cell to avoid reflection of light.

Because the cylindrical quartz cell was not perfectly perpendicular to the light beam, a higher noise-to-signal ratio was obtained. We improved this ratio by averaging the measured light intensity over a wavelength range of 100 nm

(101 wavelength values from 350 to 450 nm), and increased the spectrophotometer signal integration time from 0.5 to 1.8 s. These modifications produced a noise-to-signal ratio on the order of 1%. The cell had good flow stability and the intensity of light scattered from a simple colloidal dispersion was very reproducible. Mass balances performed using either colloidal particles or an inert tracer ( $\text{KNO}_3$ ), based on comparison of the injected substance mass to the total mass calculated by integration of the breakthrough curve, were always reproducible to within a few percent.

#### 3.4. Particle transport experiments

The effect of fluid flow velocity and nanoparticle concentration on the latex particles breakthrough curves was investigated in nine series of experiments conducted at three different flow rates (0.60, 0.30, and 0.15  $\text{cm}^3/\text{min}$ , corresponding to approach velocities of 0.13, 0.064, and 0.032 mm/s, respectively) and three different silica volume concentrations (3, 1.5, and 0.6%). Each series, consisting of a calibration measurement plus three specific experiments (to be described later), was performed on the same day with the same flow rate, silica concentration, and porous bed, packed immediately before the series. A reference UV/Vis absorption measurement (blank) was always made immediately before calibration and for every experiment. The temperature was kept at  $23 \pm 1^\circ\text{C}$  and the solution pH was maintained at 10 during all experiments to minimize deposition of the polystyrene particle onto the collector beads.

Calibration of the spectrophotometer was conducted using three different concentrations of a freshly prepared latex particle suspension. The three samples were produced by 4-, 8-, and 16-fold dilution of the initial suspension, and the resulting absorbance readings spanned the range of readings observed in the actual transport experiments. The absorbance was found to be proportional to polystyrene concentration with a proportionality coefficient of approximately 370  $\text{mg}/(\text{l.a.u.})$  and a standard deviation lower than 1%. Note that because of small changes in the concentration of polystyrene particles used in the calibration samples, this proportionality constant varied slightly from one experimental series to the next; however, the deviation was never greater than 20%. It should be noted that this was not of great concern, since our interest was not in the absolute number of latex particles exiting the bed but rather the change in the number of particles produced by the addition of the silica nanospheres. The absorbance measured over a period of approximately 5 min for every polystyrene concentration was stable, indicating that polystyrene aggregation was negligible. Immediately after calibration, the packed column was connected to the pump and tubing system and the transport experiments were conducted.

We observed in our studies that the properties of the packed bed changed slightly from one series to the next. Because of this, the first experiments in each series consisted of

measuring the transport behavior of the polystyrene colloidal particles in the absence of any depletion interaction (i.e., no silica nanoparticles present) to obtain a reference breakthrough curve. After equilibration of the system, a pulse of the polystyrene suspension was injected into the background electrolyte (KOH plus KCl) to initiate the particle transport experiment. Due to the very small amount of the injected polystyrene suspension, its effect on solution pH or ionic strength can be neglected. Obviously, local decreases in ionic strength and pH no doubt occurred at the point of injection, but these changes had no significant effect on polystyrene aggregation in solution due to the large particle–particle repulsive energy barrier. Further, due to the relatively high ion diffusion rate and effective mixing of the suspension at the column inlet, these local effects could be neglected. Once the column outlet particle concentration became negligible (typically after 1.9 pore volumes), the background electrolyte was switched to deionized water to estimate the amount of reversibly adsorbed polystyrene. This experiment was continued for additional 2.2 pore volumes.

The second experiment in each series was designed to investigate the transport behavior of the colloidal particles in the presence of a depletion interaction. The starting background solution was a silica suspension with predetermined aliquots of potassium chloride (KCl) and 1 M potassium hydroxide (KOH) stock solutions added to adjust the pH to 10 and the ionic strength to 10 mM. After equilibration of the system, a pulse of the polystyrene suspension was injected into the background silica suspension to initiate the particle transport experiment. After 2.9 pore volumes, when the measured column effluent absorbance became negligible, the background suspension was switched to an electrolyte solution with the same solution pH and ionic strength but no silica nanoparticles. This eliminated the depletion interaction without any change in the electrostatic and van der Waals forces, allowing particles attached to the collector surface in the secondary minimum to be released from the bed. For experiments where the depletion interaction effect was sufficiently strong, we observed an absorbance peak in the bed effluent, indicating a sudden release of latex particles from the bed. Finally, when the colloid concentration again became very low (after 5.1 pore volumes), the background electrolyte was switched to deionized water to estimate the amount of polystyrene still remaining in the bed. Typically a small absorbance peak was detected. The experiment was continued until the particle concentration of the column effluent eventually reached zero (after a total of 7.3 pore volumes).

The concentration of silica nanoparticles used to produce the depletion interaction was high enough to contribute slightly to the measured absorbance. We thus performed a final experiment in every series to measure this contribution and correct the absorbance from the polystyrene/silica mixtures. This experiment was conducted in exactly the same way as the second one (i.e., the background solution contained the silica particles) but we injected deionized water

instead of the polystyrene suspension to the loop. (DI water was used to simulate the slight dilution of the silica suspension produced by the injected pulse.) Absorbance values measured in this experiment were subtracted from values obtained in the second experiment to determine the scattering effect resulting from the polystyrene particles alone.

In addition to the nine series discussed above (three silica concentrations at three different flow rates), two other series of experiments were performed to measure the effect of residence time and flow rate. These series used a silica volume concentration of 3% and an approach velocity of 0.032 mm/s ( $Q = 0.15 \text{ cm}^3/\text{min}$ ). The first of these series was conducted as described above but the porous bed length was reduced to 7.4 cm. Because a shorter column resulted in a longer tailing in the breakthrough curve, we changed the background switching time to 2.3 pore volumes in the first experiment and to 4.6 and 8.6 in the second and third experiments of the series. This produced a total time of the first experiment of 4.5 pore volumes, and 12.7 pore volumes for the second and third experiments.

The other additional series, composed of two experiments, was designed to test the effect of a controlled increase in flow rate. The first experiment in this series was conducted in the same manner as described above (i.e., breakthrough in the absence of added silica nanoparticles). In the second experiment, however, the background silica suspension was not removed. Instead, the flow rate was increased every 8 s by about 10%, starting with a velocity of 0.032 mm/s ( $Q = 0.15 \text{ cm}^3/\text{min}$ ) at 2.4 pore volumes and increasing to a velocity of 0.13 mm/s ( $Q = 0.60 \text{ cm}^3/\text{min}$ ) at 2.7 pore volumes. The experiment was continued until 7.1 pore volumes when the measured light intensity reached its final level.

Finally, we performed several tests to check that our experimental setup yielded reproducible results and accurate mass balances. These tests were performed by injecting a pulse of either an inert tracer (2 mM  $\text{KNO}_3$ ) or a colloidal suspension of polystyrene latex particles in the 14.8 cm long bed. For the tests with the polystyrene particles, the solution pH and ionic strength were the same as those used in the actual experiments, and the flow rates used in both the tracer and colloidal suspension tests were the same as those in the above experiments. All tests were continued for three pore volumes to allow the measured absorbance values to return to their background values and each test was repeated.

#### 4. Results

In this section we present the measured particle breakthrough curves. Note that all points in the figures represent experimental data (normalized concentration versus pore volume) with no fitting. In all figures the recovery,  $\eta$ , is calculated as  $\eta = 100\% m_i/m_1$ , where  $m_i(t_f) = Q \int_0^{t_f} c(t) dt$  is the total mass of tracer or polystyrene particles detected during measurement until time  $t_f$ . Here  $c$  is concentration,  $t$  is

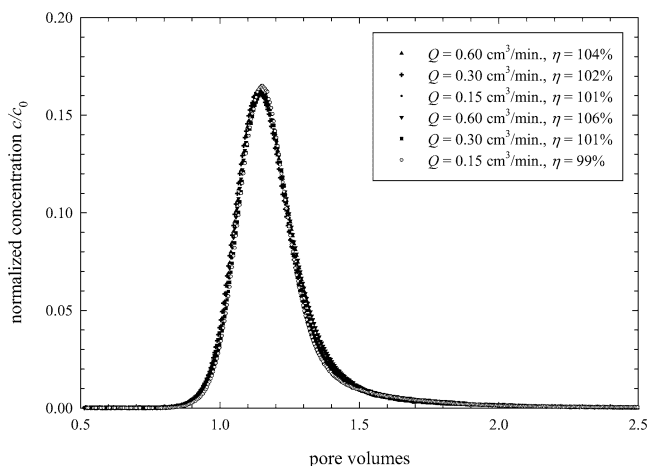


Fig. 4. Colloid elution profiles at different flow rates with no added silica nanoparticles (control runs).

time,  $Q$  is volumetric flowrate, and  $m_1$  is total mass of tracer or polystyrene particles injected to the loop.

#### 4.1. Verification of the flowthrough cell

As noted above, a series of experiments were performed with either an inert tracer or a suspension of polystyrene particles to test the system mass balance and reproducibility with the custom-made flowthrough cell. Tracer breakthrough curves were very smooth, the total recovery was always equal to 98–99%, and the reproducibility of the results was very good. The latex particle transport behavior through the packed bed column at flow rates of 0.15, 0.30, and 0.60  $\text{cm}^3/\text{min}$  (two measurements at each flow rate) is depicted in Fig. 4. All the profiles are smooth and very reproducible. The nearly identical shape of the curves suggests that the hydrodynamic dispersion in the bed is essentially the same for all flow rates used. It should be noted that the polystyrene particle recovery increased slightly with flow, which may result from some mixing problems in the flowthrough cell or simply from reduced particle retention at higher flow rates.

#### 4.2. Effect of silica concentration and flow rate

Results of the nine experimental series designed to test the impact of depletion interaction on particle transport and retention are presented in Figs. 5, 6, and 7. The figures show the data obtained at volumetric flow rates of 0.60, 0.30, and 0.15  $\text{cm}^3/\text{min}$ , respectively. Graphs a, b, and c in each figure correspond to silica volume concentrations of 0.6, 1.5, and 3%, respectively. In addition, each graph shows the breakthrough for the reference experiment performed with no added silica nanoparticles. As seen, depending on the flow rate and silica concentration, one can distinguish up to three peaks in the plots, corresponding to polystyrene particles breaking through (1) in the presence of the silica nanoparticles, (2) after the removal of the silica particles and

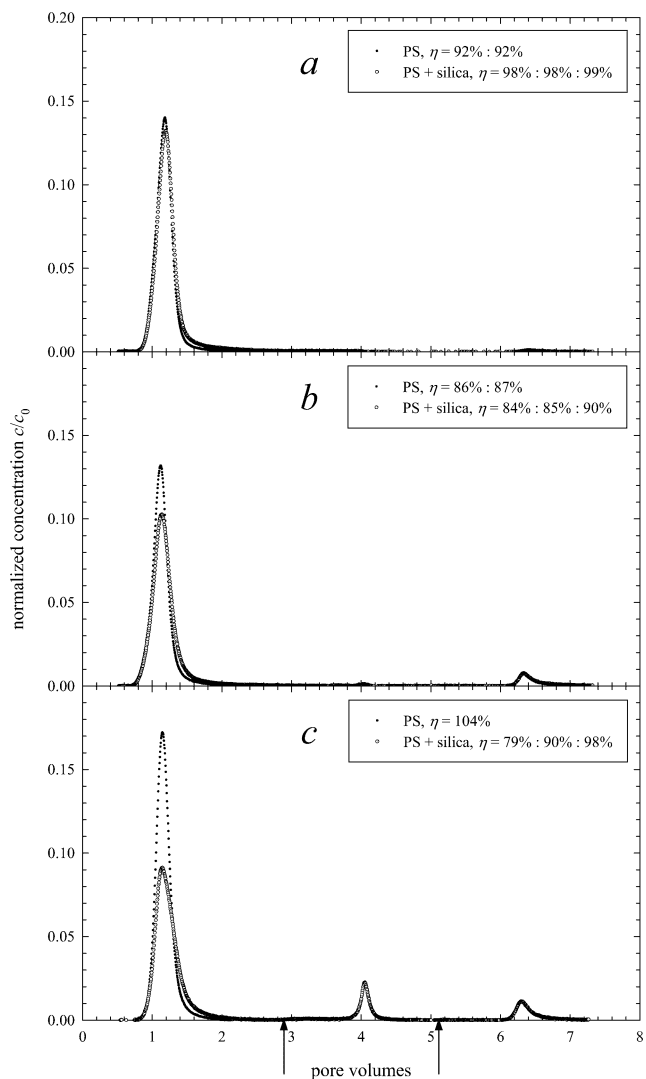


Fig. 5. Colloid elution profiles at flow rate  $Q = 0.60 \text{ cm}^3/\text{min}$ . The silica concentrations used in the graphs were: (a)  $\phi = 0.6\%$  vol, (b)  $\phi = 1.5\%$  vol, and (c)  $\phi = 3.0\%$ . In each graph, the first peak is the particle breakthrough in the presence of the silica nanoparticles, the second peak is the breakthrough resulting from replacing the silica suspension with an electrolyte solution with the same pH and ionic strength, and the third peak is the breakthrough resulting from replacing the electrolyte solution with deionized water (the arrows indicate time of switching the background solution).

flowing the background electrolyte solution, and (3) after switching from the electrolyte solution to deionized water. The value of  $\eta$  given in each graph corresponds to the cumulative particle recovery after each of these peaks. For the reference experiments (no silica nanoparticles), two reference peaks were typically observed, corresponding to the initial breakthrough in the presence of the electrolyte solution, plus a second breakthrough when the electrolyte solution was replaced with deionized water (the latter was always very small, ca. 1%). For these systems, we report the cumulative recovery value after each of these two peaks.

The effect of a depletion interaction can be seen by comparing the polystyrene particle recovery in the absence of silica nanoparticles to that obtained in the presence of

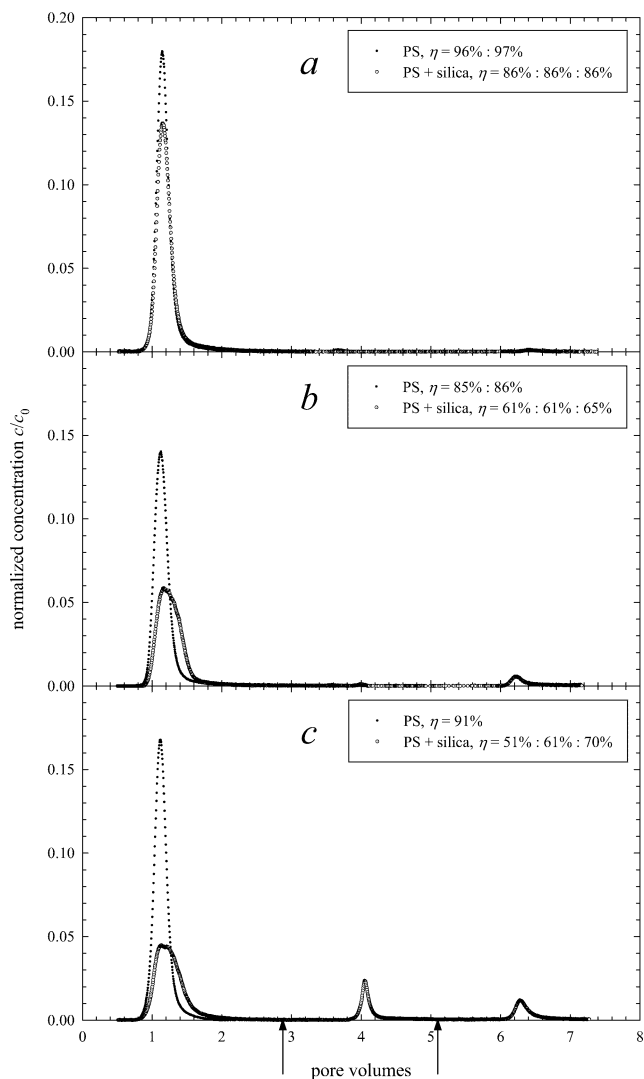


Fig. 6. Same as Fig. 5, except that the carrier fluid flow rate is  $Q = 0.30 \text{ cm}^3/\text{min}$ . The silica concentrations in graphs a–c are the same as in Figs. 5a–5c.

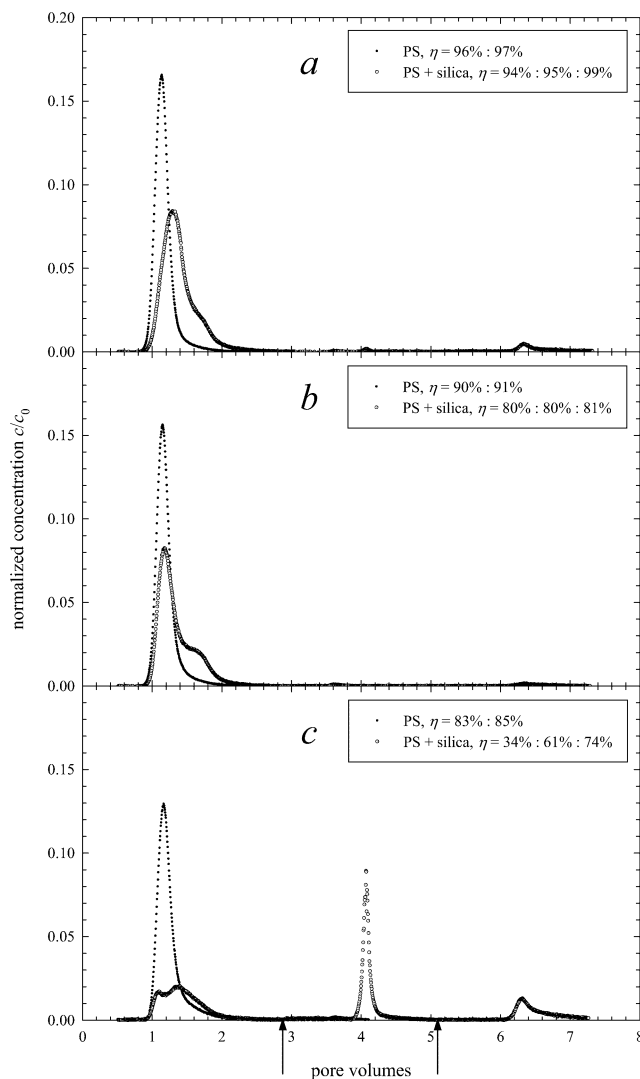


Fig. 7. Same as Fig. 5, except that the carrier fluid flow rate is  $Q = 0.15 \text{ cm}^3/\text{min}$ . The silica concentrations in graphs a–c are the same as in Figs. 5a–5c.

Table 2  
Fractional Recovery of latex particles from the breakthrough peaks in Figs. 5–7

Silica conc, % vol	Flow rate, $\text{cm}^3/\text{min}$		
	0.15	0.3	0.6
0.6	96/94	96/86	92/98
1.5	90/80	85/61	86/84
3.0	83/34	91/51	104/79

First and second values correspond to recoveries with no depletion interaction (no silica present) and with depletion interaction (silica present), respectively.

the silica. These recoveries are represented by the areas of the corresponding peaks in the graphs in Figs. 5–7 and are summarized in Table 2. For each particular flow rate and silica concentration, the first value is the percentage recovery with no added silica (experiment one of each series), while the second value is the recovery in the presence of the silica.

It is clear that, for a given flow rate, the amount of polystyrene latex particles recovered decreases as the concentration of silica increases. The flow rate also appears to have an effect on the recovery in presence of the silica nanoparticles, such that the recovery is generally higher at the higher flow rates; however, this trend is clearly not observed with the 1.5% silica concentration. These trends are discussed in greater detail in the following section.

## 5. Discussion

### 5.1. Predicted interaction energy profiles

Describing the particle transport and retention behavior in our system in a rigorous, theoretical manner would be extremely difficult. One reason for this difficulty is the fact that the depletion-induced deposition is a reversible process in-

volving secondary energy wells. Since such secondary wells occur at relatively large separation distances from the surface, particles captured in such wells are likely mobile and can thus translate along the collector surface, in addition to attaching, detaching, and reattaching to the collectors. Such a process could clearly lead to vastly different transport pathways (i.e., bulk convection versus “jumping” between collector beads). Also, due to the rapid change in colloid concentration at the peak area and relatively slow accumulation of particles at the secondary well, an exact analysis of particle transport is very cumbersome. In addition, because the attractive depletion force is relatively weak, the hydrodynamic drag force exerted on particles trapped near the surface may contribute significantly to the detachment rate. Predicting this contribution would be difficult, as the drag force will vary both with the separation distance between the particle and the collector and the position of the particle on the spherical collector surface. Finally, it is well known that the surface charge density on the surface of the glass collector beads may be heterogeneous, which can have a significant effect on the rate of particle attachment and detachment. (These last two effects are discussed further below.) Thus, rather than attempting a rigorous description, we will analyze the process qualitatively using the predicted equilibrium potential energy profiles.

Since the pH and ionic strength of all solutions were fixed, the equilibrium energy profiles are functions only of the concentration of the silica nanoparticles. The profiles for the 0.6, 1.5, and 3.0% vol concentrations used in the experiments are shown in Fig. 8. Because of the strong electrostatic repulsion between the like-charged latex particles and the glass bead collectors, the barrier to primary, irreversible deposition is very large and can be considered infinite. With no added silica nanoparticles, little, if any, secondary well is predicted, meaning that no particle deposition should occur. At silica concentrations of 0.6, 1.5, and 3.0%, secondary en-

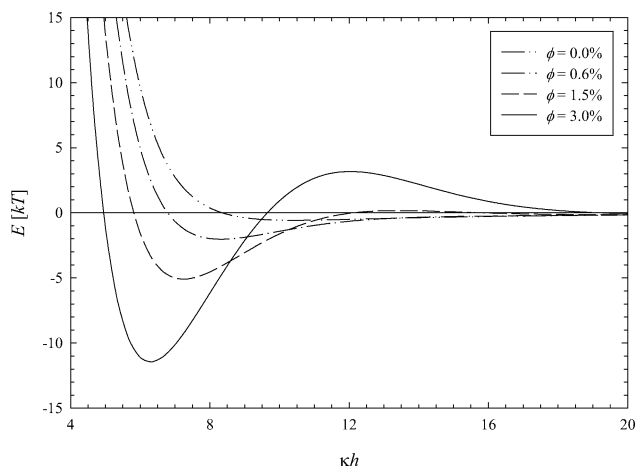


Fig. 8. Colloid particle–collector interaction profiles based on Eq. (1) at three different values of the depletant concentration. The specific parameters used here were those corresponding to the experimental system (see Table 1). The dash-dot-dot line shows the DLVO profile.

ergy wells of 2, 5, and 11  $kT$ , respectively, are formed. The location of the wells varies from 25 nm ( $\kappa h = 8.3$ ) in the 0.6% silica system to 19 nm ( $\kappa h = 6.3$ ) in the 3.0% system. In the 3.0% system, a secondary barrier of approximately  $3kT$  is also predicted. As discussed by various authors (see, for example, [9,13,28–30]), this barrier results from ordering of the nanoparticles in the gap region. Sharma et al. [31] showed that at sufficiently high nanosphere concentrations, this barrier can actually become large enough to stabilize a system against secondary flocculation (typically termed depletion restabilization). The  $3kT$  barrier predicted here, however, would not be sufficient to produce such restabilization.

## 5.2. Relating transport behavior to potential energy profiles

A particle moving through the bed in the presence of the nonadsorbing silica particles that comes sufficiently close to a collector surface can enter the secondary energy wells shown in the potential profiles in Fig. 8. For the systems in which the energy well is only several  $kT$  in depth, such as the well at the lowest silica concentration, the probability of detachment will be relatively high. Note that the probability of detachment scales roughly as  $\exp(-E_{\text{well}}/kT)$ , where  $E_{\text{well}}$  is the depth of the secondary energy well. Thus, after a relatively short time spent at the collector surface the particle will continue to travel through the bed. Because of the finite time spent in the well, though, the effective particle transport rate would be slower in the presence of secondary energy wells. In addition, because of the stochastic nature of the deposition and detachment process, the breakthrough pulse should be wider. However, the particle recovery in the first pulse should still be near 100%.

The breakthrough curves in Figs. 5a, 6a, and 7a (summarized in Table 2) clearly support the trend discussed above. This is especially evident in Fig. 7a, where the first peak is substantially broader in the presence of the silica particles, yet the total recovery is still 94%. Moreover, the results at the lowest flow rate (Fig. 7) suggest that a relatively sizeable fraction of latex particles undergoes deposition in the secondary minimum. In this case, the bimodal shape of the particle breakthrough curve suggests two populations of particles traveling through the column. The location of the first maximum corresponds to the location of the peak obtained without any depletion interaction. Thus, the first particle population exiting the column comprises particles which did not interact with the collector surface. We theorize that the second population exiting the column, at about 0.3 pore volumes later, results from particles that interacted with the collector surface and, consequently, had a longer residence time in the column. As one can see in Fig. 7, the bimodal character of the particle concentration profile (first peak) is more discernable at higher silica concentrations, where the secondary energy well is deeper. For the latter, the ratio of retarded to freely traveling particle populations increases due to the longer time needed for the detachment process.

When the energy wells are sufficiently large, however, such as greater than  $10kT$ , the probability of a particle detaching from the secondary well becomes small enough that the capture can be considered effectively irreversible. For this case, the particle recovery in the first outlet peak would be substantially less than 100%. In addition, when the silica particles are removed, eliminating the secondary well, the captured particles would be released and the cumulative recovery for the first two peaks should be, in principle, near 100%. Again, this trend can be seen in Figs. 5c, 6c, and 7c. Especially noticeable here is the additional recovery obtained upon removing the silica particles, which is not observed at the lower silica concentrations. It should be noted, also, that despite the deep secondary minimum at the highest silica concentration, the bimodal character of the first peak in Fig. 7c, corresponding to the lowest flow rate, is clearly visible. This suggests that reversible (short-time) deposition of the latex particles also takes place at the highest silica concentration. This is most likely due to collector surface heterogeneity, which results in modification of the predicted interaction energy profile and the secondary energy well depth.

While the trends observed in the measured breakthrough curves are consistent with the predicted energy profiles, it is also apparent that significant discrepancies arise when attempting a more quantitative comparison. For example, in Figs. 6c and 7c, the cumulative recovery obtained even after the silica particles are removed is still much less than 100%. We attribute these discrepancies to the presence of surface charge heterogeneities. For example, if the charge density on the glass collector beads is not uniform, the added depletion attraction could be sufficient to overcome the primary energy barrier in regions where the charge density is low, thus allowing deposition into the deep primary minimum. Because of the strong van der Waals attractive force, particles in the primary minimum would not be released upon removing the silica nanoparticles, and they could even remain attached upon replacing the electrolyte solution with deionized water (i.e., increasing the strength of the electrostatic repulsion). This would explain the relatively low cumulative recoveries in all three peaks seen in Figs. 6c and 7c. The impact of collector surface charge heterogeneity on particle transport in packed columns has been investigated by numerous researchers [32] and is thought to be the reason for the finite deposition observed even in systems where the particle-collector interaction is predicted to be strongly repulsive.

Another contributing cause could be the local variability in the charge on the latex particles as well as the distribution in the charge density of the particles themselves. As seen in Table 1, the standard deviation in the measured zeta potential, 15 mV, was approximately 14% of the mean value. This variability could result in the more highly charged particles passing through the bed and the lower charged particles becoming captured in the primary minimum.

### 5.3. Residence time vs flow rate effects

The graphs in Figs. 5–7 clearly indicate that at a fixed concentration of silica nanoparticles, the flow rate through the packed bed has also a pronounced effect on the transport and retention behavior of the latex particles. In general, in the presence of the silica nanoparticles, increasing the flow rate reduces the number of particles that remains deposited in the bed. Two possible explanations for this observation were explored. First, the smaller number of captured particles could simply result from the smaller residence time in the column (i.e., fewer chances for the particles to interact with the collector beads). Second, the higher velocities could exert a greater hydrodynamic drag force on the captured particles. Hence, it is possible that the greater breakthrough resulted from hydrodynamic facilitated release of latex particles from the secondary energy wells. The latter should affect not only the particle recovery, but also the shape of the particle breakthrough curves.

To test the relative contributions of these two effects, we ran two additional series of experiments (described earlier in Section 3.4). The first series used the same conditions as those in Fig. 7c (i.e., 3% silica and  $0.15 \text{ cm}^3/\text{min}$  flow rate), except that the length of the packed bed of glass beads was reduced from 14.8 to 7.4 cm. This means that the hydrodynamic conditions in the bed remained essentially the same as in Fig. 7c, while the residence time in the bed was reduced by half. The results of this first series are shown in Fig. 9. As seen, the particle recovery in the first peak increased from 34 to 56% (meaning that fewer particles remain captured), while the recovery in the second peak (upon removal of the silica) decreased from 27 to 17% (again indicating that fewer particles were captured). Clearly the residence time of the particles in the column is an important parameter in determining the fraction of particles that remain captured.

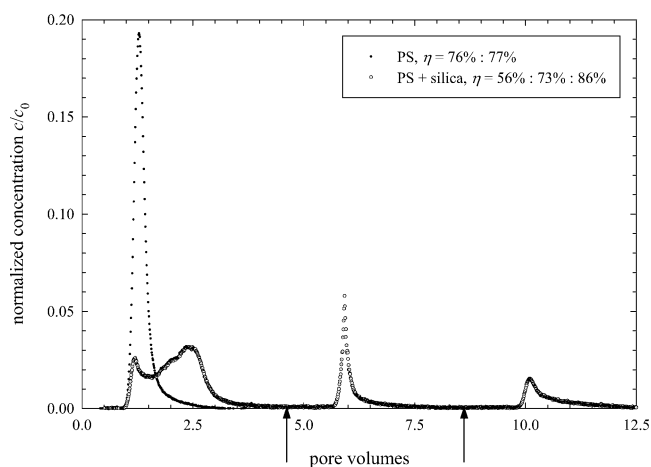


Fig. 9. Colloid elution profile at flow rate  $Q = 0.15 \text{ cm}^3/\text{min}$  and silica concentration  $\phi = 3\%$  with a 7.4-cm-long column. Arrows indicate time of switching the background solution.

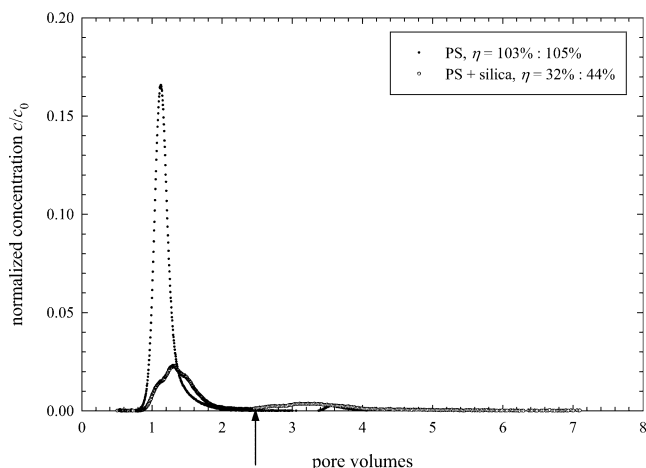


Fig. 10. Effect of flow rate increase on colloid elution profile at silica concentration  $\phi = 3\%$ . For the experiment with silica particles, the volumetric flow rate was kept at  $0.15 \text{ cm}^3/\text{min}$  up to 2.4 pore volume. Between 2.4 and 2.7 pore volumes, the volumetric flow rate was slowly increased (increases of approximately 10% every 8 s) up to a final flow rate of  $0.60 \text{ cm}^3/\text{min}$ . Arrow indicates time of switching the flow rate.

The second experimental series was designed to test the effect of the bulk fluid velocity on the particle deposition/detachment process. As described above, the first experiment of this series was performed exactly the same as that shown in Fig. 7c (i.e., 3% silica and a flow rate of  $0.15 \text{ cm}^3/\text{min}$ ). In the second step, however, rather than removing the silica nanospheres, the bulk flow rate was increased to  $0.60 \text{ cm}^3/\text{min}$ . As seen in Fig. 10, 32% of the initially injected particles were recovered in the first peak, which agrees well with the 34% recovery obtained under identical conditions in Fig. 7c. However, when the flow rate was increased to  $0.60 \text{ cm}^3/\text{min}$ , an additional recovery of 12% was obtained. These newly released particles were captured in the bed at the lower flow rate, indicating clearly that the drag force on the captured particles produced by the moving fluid is significant enough to affect their release.

In summary, these additional results show that both the residence time and the velocity in the column are important factors in determining the fraction of particles captured in the bed. Furthermore, in addition to the effect of flow rate on particle retention (recovery), it is quite discernable that the shape of the breakthrough curves is generally influenced by the flow rate.

## 6. Concluding remarks

The experiments presented in this paper clearly demonstrate that secondary energy wells produced by a depletion attraction can have a marked effect on the transport and retention behavior of particles traveling through a bed of like-charged collectors. At low nonadsorbing nanoparticle concentrations, where the secondary energy well is only a few  $kT$ , a fraction of the particle population undergoes slower transport compared to the case of a purely repulsive

particle-collector interaction; however, very few particles remain captured in the bed in this case (i.e., the deposition is completely reversible). The observed bimodal shape of the particle breakthrough curves, especially at lower flow rates, suggests two pathways for particle transport—a fast bulk transport of particles and a slower transport of particles affected by the secondary energy well. However, when the secondary well becomes on the order of  $10kT$  or more, which occurs upon increasing the nanoparticle concentration, a significant fraction of the particles remains captured in the secondary energy well. Upon removal of the silica nanoparticles and eliminating the secondary well, many of these captured particles are released. The fraction of particles remaining captured in the bed was also found to be an increasing function of the particle residence time in the bed and, separately, a decreasing function of the carrier fluid velocity. This latter dependence suggests that the hydrodynamic drag force exerted on particles captured in secondary energy wells can be sufficient to enhance their release.

## Acknowledgments

P.W. thanks Martin Piech and Arthur Hersel in the Department of Chemical Engineering at Yale for helpful discussions. The authors also acknowledge the assistance of Dr. Andrei Dukhin of Dispersion Technology, Inc., for help in characterizing the silica nanoparticles with acoustic and electroacoustic spectroscopy. This work was supported by the U.S. National Science Foundation (Grant CTS-9912098).

## References

- [1] S. Asakura, F. Oosawa, *J. Chem. Phys.* 22 (1954) 1255.
- [2] J.E. Seebergh, J.C. Berg, *Langmuir* 10 (1994) 454.
- [3] P. Jenkins, M. Snowden, *Adv. Colloid Interface Sci.* 68 (1996) 57.
- [4] P. Richetti, P. Kekicheff, *Phys. Rev. Lett.* 68 (1992) 1951.
- [5] S. Biggs, J.L. Burns, Y.D. Yan, G.J. Jameson, P. Jenkins, *Langmuir* 16 (2000) 9242.
- [6] A.J. Milling, K. Kendall, *Langmuir* 16 (2000) 5106.
- [7] A.J. Milling, *J. Phys. Chem.* 100 (1996) 8986.
- [8] A.J. Milling, S. Biggs, *J. Colloid Interface Sci.* 170 (1995) 604.
- [9] D. Rudhardt, C. Bechinger, P. Leiderer, *J. Phys. Condens. Matter.* 11 (1999) 10073.
- [10] P.C. Odiachi, D.C. Prieve, *Colloids Surf. A* 146 (1999) 315.
- [11] E.S. Pagac, R.D. Tilton, D.C. Prieve, *Langmuir* 14 (1998) 5106.
- [12] A. Sharma, S.N. Tan, J.Y. Walz, *J. Colloid Interface Sci.* 191 (1997) 236.
- [13] A. Sharma, J.Y. Walz, *J. Chem. Soc. Faraday Trans.* 92 (1996) 4997–5004.
- [14] D.L. Sober, J.Y. Walz, *Langmuir* 11 (1995) 2352.
- [15] P.K. Thwar, D. Velegol, *Langmuir* 18 (2002) 7328.
- [16] J.C. Crocker, J.A. Matteo, A.D. Dinsmore, A.G. Yodh, *Phys. Rev. Lett.* 82 (1999) 4352.
- [17] M. Piech, P. Weroński, X. Xu, J.Y. Walz, *J. Colloid Interface Sci.* 247 (2002) 327.
- [18] J.Y. Walz, A. Sharma, *J. Colloid Interface Sci.* 168 (1994) 485.
- [19] M. Piech, J.Y. Walz, *J. Colloid Interface Sci.* 225 (2000) 134–146.

- [20] M. Piech, J.Y. Walz, *J. Colloid Interface Sci.* 232 (2000) 86–101.
- [21] G.M. Bell, S. Levine, L.N. McCartney, *J. Colloid Interface Sci.* 33 (1970) 335.
- [22] V.A. Parsegian, G.H. Weiss, *J. Colloid Interface Sci.* 81 (1981) 285.
- [23] P. Weronki, J.Y. Walz, *J. Colloid Interface Sci.*, in press.
- [24] A.S. Dukhin, P.J. Goetz, *Adv. Colloid Interface Sci.* 92 (2001) 73.
- [25] R.W. O'Brien, L.R. White, *J. Chem. Soc. Faraday Trans. II* 74 (1978) 1607.
- [26] A.E. Childress, M. Elimelech, *J. Membr. Sci.* 119 (1996) 253.
- [27] R. Kretzschmar, K. Barmettler, D. Grolimund, Y. Yan, M. Borkovec, H. Sticher, *Water Resour. Res.* 33 (1997) 1129.
- [28] B. Groh, S. Dietrich, *Phys. Rev. E* 59 (1999) 4216.
- [29] D. Henderson, M. Loszda-Cassou, *J. Colloid Interface Sci.* 114 (1985) 180.
- [30] B. Götzelmann, R. Evans, S. Dietrich, *Phys. Rev. E* 57 (1998) 6785.
- [31] A. Sharma, S.N. Tan, J.Y. Walz, *J. Colloid Interface Sci.* 190 (1997) 392.
- [32] L. Song, P.R. Johnson, M. Elimelech, *Environ. Sci. Technol.* 28 (1994) 1164.